Journal of
Composites Science

MDPI

Article

Characterization of Mechanical Performance of Composites Fabricated Using Innovative Carbon Fiber Wet Laid Process

Hicham Ghossein [1,2,*], Ahmed Arabi Hassen [3], Seokpum Kim [4], Jesse Ault [5] and Uday K. Vaidya [1,4]

1 Department of Mechanical, Aerospace and Biomedical Engineering, Fibers and Composites Manufacturing Facility (FCMF), University of Tennessee, Knoxville, TN 37916, USA; Uvaidya@utk.edu
2 Endeavor Composites, Inc., Knoxville, TN 37932, USA
3 Materials Science and Technology Division (MSTD), Oak Ridge National Laboratory (ORNL), Oak Ridge, TN 37830, USA; hassenaa@ornl.gov
4 Energy and Transportation Science Division (ETSD), Oak Ridge National Laboratory (ORNL), Oak Ridge, TN 37830, USA; kimsp@ornl.gov
5 School of Engineering, Brown University, Providence, RI 02912, USA; jesse_ault@brown.edu
* Correspondence: Hghossein@endeavorcomposites.com

Received: 28 July 2020; Accepted: 18 August 2020; Published: 22 August 2020

Abstract: Recent innovation in production of optimized nonwoven wet laid (WL) carbon fiber (CF) mats raised the question of optimal translation of the performance and isotropy into composites formed through these dry preforms. This work explores the mechanical behavior of composites produced from WL-CF mats in conjunction with the microstructure predicted through Object Oriented Finite Element Analysis (OOF). The mats used for the composites were prepared in two dispersion regimes using 25.4 mm long CF. The mixing regimes discussed in the author's previous work, are identified as Method 1 for the traditional processing regime and Method 2 for the innovative regime that provided optimal nonwoven WL-CF mats. Composite panels from Method 2 mats showed a normalized tensile strength increase of 52% over those from Method 1 panels. Reproducibility analysis of composites made from Method 2 mats demonstrated a standard deviation of 2% in fiber weight content, 2% in tensile modulus and 9% in tensile strength, while composites made from Method 1 mats demonstrated a standard deviation of 5% in fiber weight content, 5% in tensile modulus and 17% in tensile strength. Systematic study of the microstructure and its analysis through OOF confirmed the isotropy translation of mats produced through method 2 to the composites. This study validated the hypothesis that optimal nonwoven mats lead to a well-balanced composite with optimal performance and that non-optimal nonwoven mats do not pack into a well-balanced composite.

Keywords: wet laid; isotropic; tensile; carbon fiber; discontinuous

1. Introduction

Recent environmental issues related to global climate change and greenhouse gas emissions have prompted automotive manufacturers to focus on the development of lightweight and fuel efficient vehicles [1]. Fiber reinforced composites possess the advantage of high strength-to-weight and stiffness-to-weight ratios, light weight, low fatigue susceptibility and superior damping capacity [2–4].

The authors in their previous work [5] explored the production of nonwoven CF wet laid (WL) mats through two methods of fiber dispersion. Method 1 used a shear mixer to spread the fiber bundles, but it resulted in an unequal fiber distribution in the mats with somewhat inconsistent reproducibility. Method 2 used an innovative mixer based on chaotic advection theory which provided a fully balanced

fiber distribution and consistent reproducibility of the mats. Researchers [6–10] have shown that porous nonwoven fabrics like the nonwoven WL-CF mats possess high specific surface area, light weight and ease of processing into complex geometries. This study investigates the mechanical properties of composite plates produced from nonwoven CF-WL mats made through Method 1 and Method 2. The experimental mechanical properties of both types of composites are provided within this paper. Further, a microstructure based finite element analysis (FEA) has been conducted on the mats made by each of the two methods to determine the effect on the mechanical properties of the final composite.

The effect of microstructure on mechanical properties of a composite is well explored. Straumit et al. [11] used X-ray computed tomography to quantify the internal structure of textile composites using an automated voxel model. Wan et al. [12] investigated the tensile and compressive properties of chopped carbon fiber tapes with respect to the changes in microstructure based on tape length and molding pressure. The authors found that increasing structural integrality improved the composite mechanical properties. In a second study, Wan et al. [13] analyzed the microstructural differences in CF composites using X-ray micro-CT. This method provided information on the morphology of the composite which was used to predict its mechanical properties. Tseng et al. [14] conducted numerical prediction of fiber orientation to predict mechanical properties for short/long glass and carbon fiber reinforced composites. Their model came within a 25% variance to the experimental data. Feraboli et al. [15] compared performance of different microstructures of various materials like recycled CF fabric/epoxy composites, twill laminates and sheet molding compounds (SMC). Similar mechanical properties were exhibited by the twill laminates and SMC under similar microstructural conditions. Caba et al. [16] characterized the fiber-fiber interactions in carbon mat thermoplastics (CMT) produced through the WL technique. Their study established a foundation for understanding the relation between the fiber volume fraction and the mechanical behavior of the composites. Evans et al. [17] proposed directed fiber compounding (DFC),producing a material similar to SMC via an automated spray deposition process of CF. They reported tensile stiffness and strength values of 36 GPa and 320 MPa for isotropic materials at 50% fiber volume. Selezneva et al. [18] investigated the mechanical properties of randomly oriented strand thermoplastic composites in an effort to quantify the effect of strand size and found that properties are dependent on the strand length. Amaro et al. [19] stated that the elastic modulus, tensile strength, and impact resistance of fiber composites increase as fiber length increases. Thomason [20] investigated the influence of fiber length and concentration on the properties of reinforced composites, and reported that above a critical fiber length (l_c), the full reinforcing potential of the reinforcement is realized due to higher fiber aspect ratio. The nonwoven WL-CF mats used in this study are produced using a 25.4 cm long CF. In order to avoid the complexity and vast data produced with X-Ray tomography to analyze the microstructure, this study refers to simpler image analysis techniques with higher precision.

Langer et al. [21] introduced an image based finite element analysis software, a novel numerical approach called object oriented finite element (OOF). OOF is a desktop software application for studying the relationship between the microstructure of a material and its overall mechanical properties using finite element models based on real or simulated micrographs. Reid et al. [22] discussed the mathematical approach and operational method for OOF and OOF2. This novel numerical approach has been used by researchers to provide fundamental insight on expectations of mechanical properties of fiber reinforced polymeric composites [23–27]. Goel et al. [28] compared experimental results for Young's modulus of long fiber thermoplastic (LFT) against predictions based on mathematical models and OOF. They reported that the closest prediction to experimental results was achieved through the OOF software.

Building on this approach, this study (a) validated the isotropy of composites made from the nonwoven WL-CF mats produced through the two discussed methods from the author's previous work [5], and (b) evaluated the composites mechanical performance with respect to theoretical prediction from Halpin–Tsai equations [29] for oriented discontinuous reinforcements.

2. Materials and Methods

This study used un-sized chopped Zoltek™ PX35 Type 02 CF with a length of 25.4 mm, average diameter of 7 μm, specific gravity of 1.81 g/cm^3, tensile strength of 4137 MPa, and tensile modulus of 242 GPa. The matrix used was a West System epoxy 105/206 mix with a specific gravity of 1.18 g/cm^3, tensile strength of 50.33 MPa and tensile modulus of 3.17 GPa.

2.1. Sample Preparations and Experimental Setup

Two different sets of CF/epoxy plates were prepared using the vacuum assisted resin transfer method (VARTM) technique. Three 306 × 306 mm plates were produced for each set, with every plate using the same five layers laminate of nonwoven WL-CF mats. The first set was processed using Method 1 mats; the second was processed with Method 2 mats. The mats contain randomly distributed fibers as seen in Figure 1 [5]. All plates were prepared on a flat glass mold surface with a nylon vacuum bag. The setup was a de-bulked under vacuum for 30 min, the resin was degassed for 10 min and the infusion took another 10 min until all fibers were fully wetted. After resin cure, samples were collected from each plate following the layout in the schematic seen in Figure 2. The samples' distribution allowed a statistical representation from the vacuum side of the plate, the center of the plate and the resin infusion side of the plate. The three sites for sample collection allow the exploration of the effect of resin to fiber distribution on the mechanical properties of the composite. The average mechanical properties of each set were considered in the study, in order to examine the reproducibility of the composite and to understand the difference between composites made from Method 1 mats and those made using Method 2 mats.

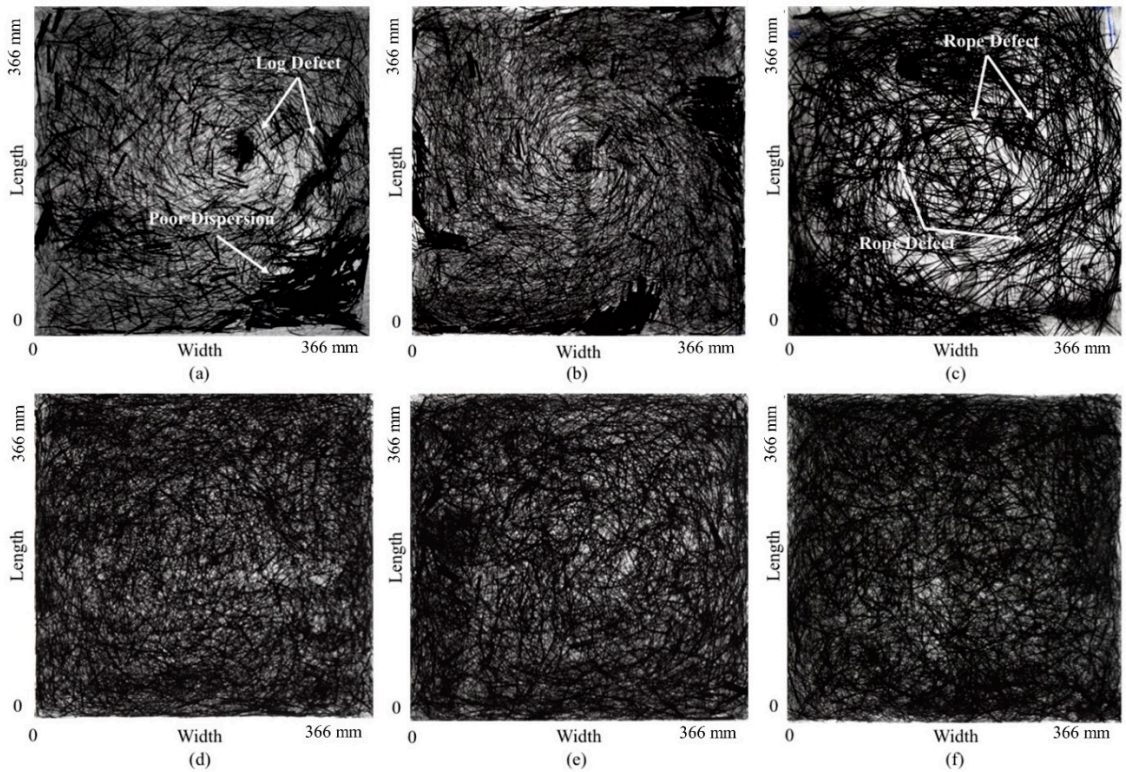

Figure 1. Back light scatter images of nonwoven wet laid carbon fiber (WL-CF) mats prepares using: (**a**) Method 1 at 10 min fiber dispersion; (**b**) Method 1 at 20 min fiber dispersion; (**c**) Method 1 at 30 min fiber dispersion; (**d**) Method 2 at 10 min fiber dispersion; (**e**) Method 2 at 20 min fiber dispersion; (**f**) Method 2 at 30 min fiber dispersion. All mats used in this study are prepared with 20 min fiber dispersion. Adopted from [5].

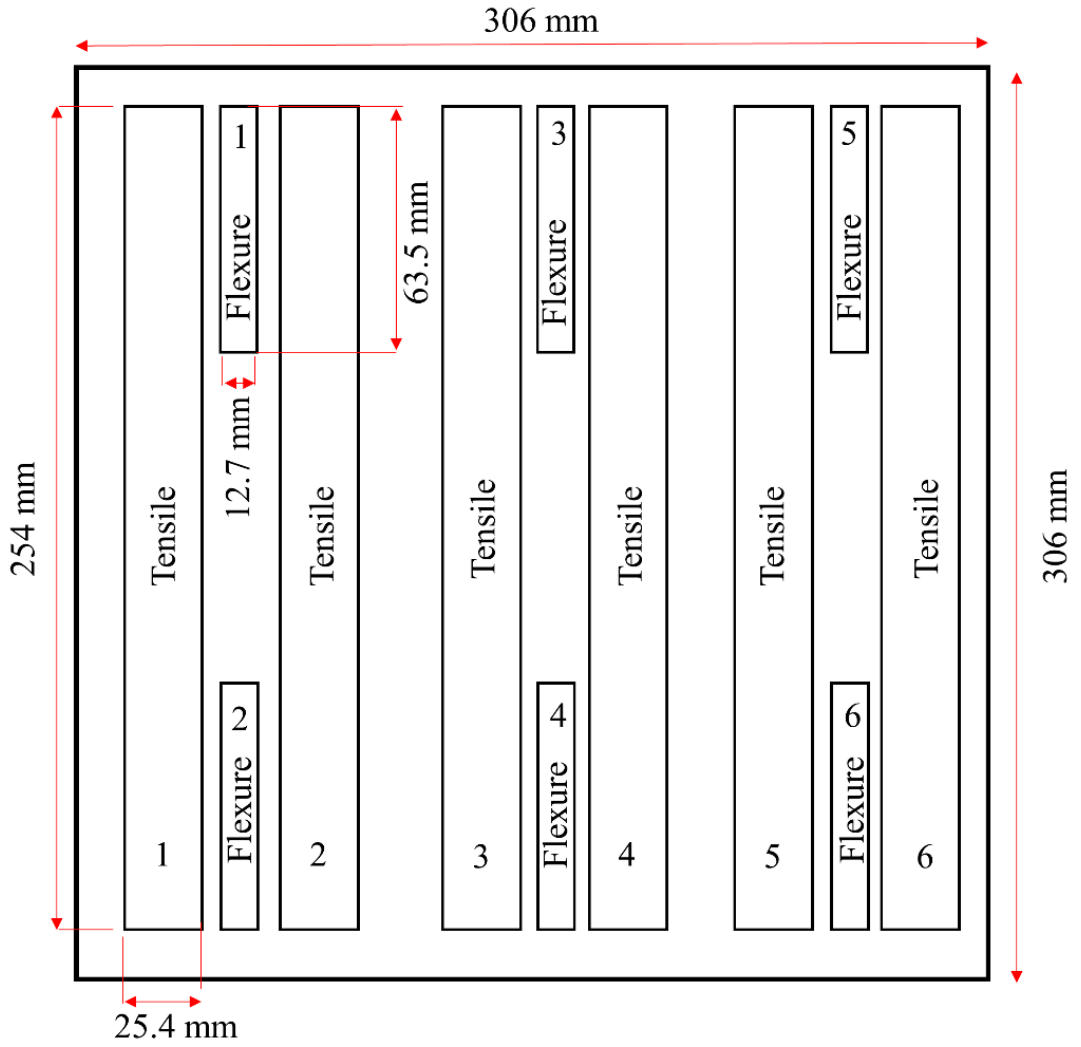

Figure 2. Location of tensile and flex samples machined from the WL nonwoven carbon fiber composite plates.

All tensile samples were tested based on ASTM D5083, all flexure samples were tested based on ASTM D790 and Inter Laminar Shear Stress (ILSS) samples were tested based on ASTM 2344. Furthermore, samples of 6.45 square cm were taken from each tensile sample for a burn off test in order to confirm the fiber weight ratio to resin distribution. All samples were weighed before and after matrix burn-off for comparison. The matrix was subjected to burn-off using a Thermo Fisher Scientific 1100 °C box furnace CF51800 series at 450 °C for three hours. Another set of 6.45 square cm samples were selected from each tensile sample for void calculations per ASTM D2734. Scanning electron microscopy (SEM) analysis was conducted to observe the break surface of the tensile samples.

2.2. Halpin-Tsai Theory and Relevance

The elastic modulus of isotropic reinforced composites is calculated theoretically by the Halpin–Tsai equations for oriented reinforcements and the Rule of Mixtures (ROM) [30]. Halpin [29] argued that it is possible to construct a material having isotropic mechanical properties from layers or plies of another or similar material. Mallick [31] stated that the Halpin–Tsai method is used to calculate the longitudinal and transverse properties of aligned discontinuous reinforcement composites, which can in turn be used to calculate the modulus of randomly oriented reinforcement composites. This study uses the Halpin–Tsai calculations to compute theoretical values for the composites under investigation by assuming the following conditions: (1) fiber cross section is circular; (2) fibers are arranged in a

square array; (3) fibers are uniformly distributed throughout the matrix; (4) perfect bonding exists between the fibers and the matrix; (5) matrix is free of voids.

For these conditions, the tensile modulus of randomly oriented discontinuous fiber reinforced composites is calculated as:

$$E_{random} = \frac{3}{8}E_L + \frac{5}{8}E_T \tag{1}$$

where E_L and E_T are the empirical longitudinal and transverse moduli, respectively, for a unidirectional discontinuous fiber reinforced composite and they are calculated as follows:

$$E_L = \frac{1 + 2\left(\frac{l_f}{d_f}\right)\eta_L v_f}{1 - \eta_L v_f}E_m \tag{2}$$

$$E_T = \frac{1 + 2\eta_T v_f}{1 - \eta_T v_f}E_m \tag{3}$$

η_L and η_T are calculated as follows:

$$\eta_L = \frac{\left(\frac{E_f}{E_m}\right) - 1}{\left(\frac{E_f}{E_m}\right) + 2\left(\frac{l_f}{d_f}\right)} \tag{4}$$

$$\eta_T = \frac{\left(\frac{E_f}{E_m}\right) - 1}{\left(\frac{E_f}{E_m}\right) + 2} \tag{5}$$

where E_m and E_f are the matrix tensile modulus and the fiber tensile modulus, respectively; and l_f is the fiber length, d_f is the fiber diameter and v_f is the fiber volume of the composite.

As for the theoretical strength, failure is predicted when the maximum tensile stress in the laminate equals the strength averaged over all possible fiber orientation angles, known as the Hahn's approach [32]. Failure is predicted when the maximum tensile stress in the laminate equals the following strength averaged over all possible fiber orientation angles:

$$S_r = \frac{4}{\pi}\sqrt{S_L S_T} \tag{6}$$

where S_r is the strength of the random fiber laminate, S_L and S_T are, respectively, the empirical longitudinal and transverse strength of a 0° laminate of continuous fibers calculated through the rule of mixture using fiber and matrix properties provided by the manufacturer.

2.3. OOF Analysis Approach with Assumption of Composites Isotropy and Its Validation

Composite microstructure has a direct influence on its mechanical properties. In order to quantify microstructural features, both morphological and material properties must be characterized. Image processing is a robust technique for the determination of morphological features.

The OOF2 software follows an adaptive meshing algorithm and specifies properties to the grid units based on pixel assignment to the material (black = Matrix, white = Fiber). Figure 3 displays polished surfaces of samples produced using a single infused nonwoven WL-CF mat from Method 1 and Method 2, showing the microstructure distribution in each samples. The use of a single mat played an important role in preventing any bias of fiber packing from multiple layers in a composite panel. A clear qualitative difference is apparent in the microstructures of the two methods. Method 1 demonstrates a higher fiber agglomeration while Method 2 has a wider fiber distribution. In both cases, a validation of the isotropic nature of the composites is required. Such validation is performed by measuring the Young's modulus in multiple directions of load application this can be done experimentally or

through computer simulation and analysis of the microstructure. Isotropy is defined by having equal Young's modulus for all load directions or a ratio of 1 when dividing the values of Young's modulus obtained from two different directions of load mounting. In this study, the microstructure performance of both methods, in different load mounting directions is evaluated through computer-simulation analysis. Using OOF2 an adaptive mesh is conformed on sample sets from each method, the mesh is then subjected to a simulated deformation through ABAQUS 2018 – HF5 to calculate the Young's modulus values for a tensile load in two principal directions.

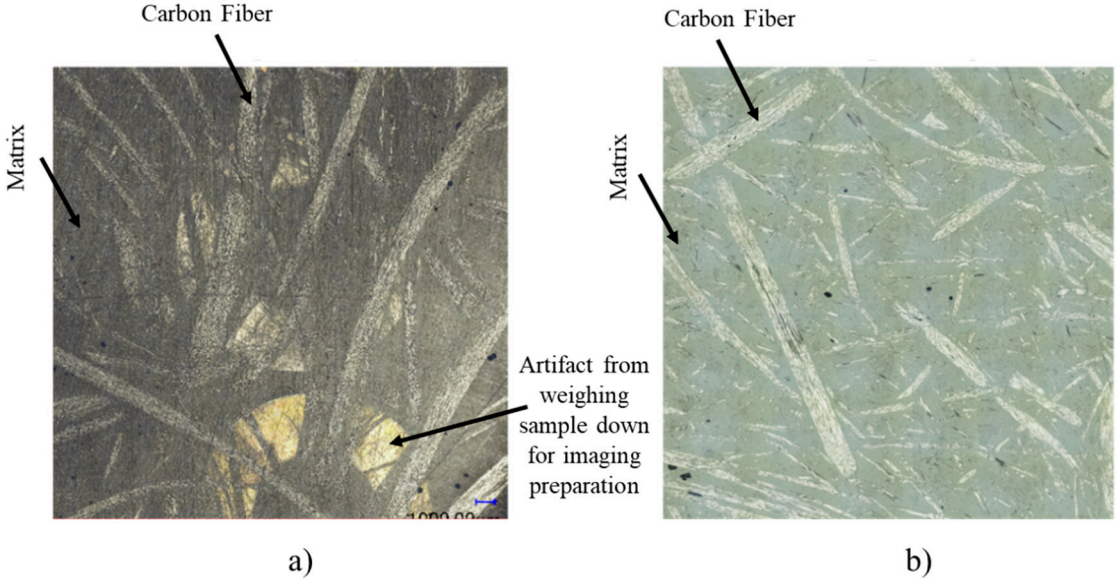

Figure 3. Polished samples showing the microstructure obtained in composite; (**a**) Micrographs for samples obtained by Method 1, and (**b**) Micrographs for samples obtained by Method 2.

The first step in this approach is to select images of a representative microstructure. Single mats prepared in similar methods to the mats shown in Figure 1b, and Figure 1e were infused with epoxy resin by the same methodology of composite preparation out of several stacked layers. Three samples per method were taken from the median of the infused mats at an area of 18 × 18 mm each. They were mounted in epoxy resin for ease of polishing, polished to reveal the microstructure and imaged at a magnification of 100×. Note that the representative image of the microstructure is somewhat subjective, thus the need for several samples for higher degree of fidelity. The samples had an average area fraction of ~33% which is representative of the overall volume fraction of fibers in the composite.

Before the OOF software is able to analyze the images and generates FEA meshes, some image processing filters need to be adopted. The constituents within the microstructure are separated into distinct grey levels through color thresholding and application of a blurring filter and contrast adjustment as seen in Figure 4. This process is similar to the approach by Goel et al. [27].

Figures 4 and 5 show the processed images with their corresponding meshes generated by OOF2 and simulated through ABAQUS for Method 1 and Method 2 sample sets, respectively. Figure 6 shows a representative microstructure and process analysis to assign a conforming mesh for the FEA processing. The area fraction of the samples is close to 33% with some variations. The samples from Method 1 showed higher variance in area fraction which reflected on the FEA results, while samples from Method 2 had higher consistency. This reflects the optimal fiber distribution of Method 2 versus the non-optimal fiber distribution of Method 1 as discussed in [5].

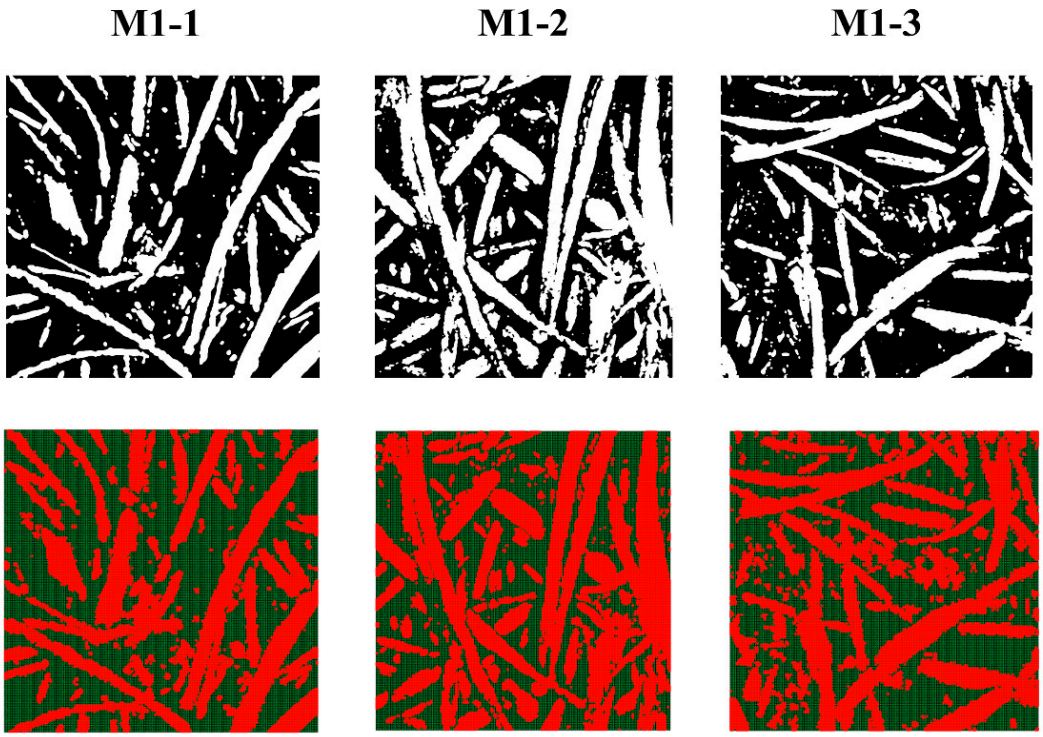

Figure 4. Method 1 modified images and their respective generated finite element analysis (FEA) meshes. M1-1 stands for Method 1-Sample 1.

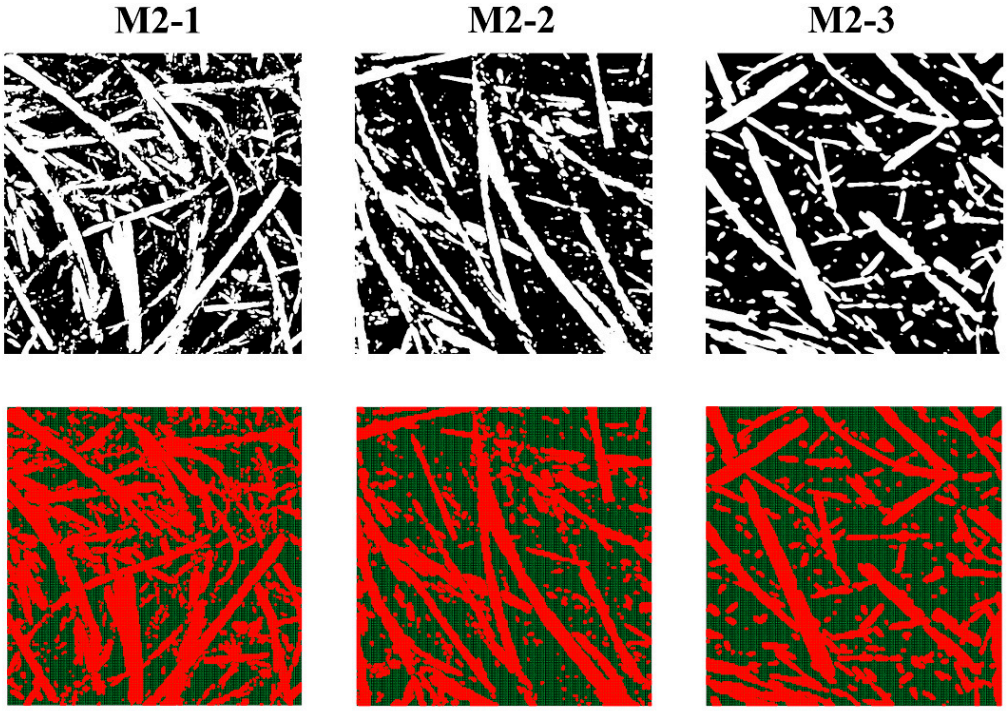

Figure 5. Method 2 modified images and their respective generated FEA meshes. M2-1 stands for Method 2-Sample 1.

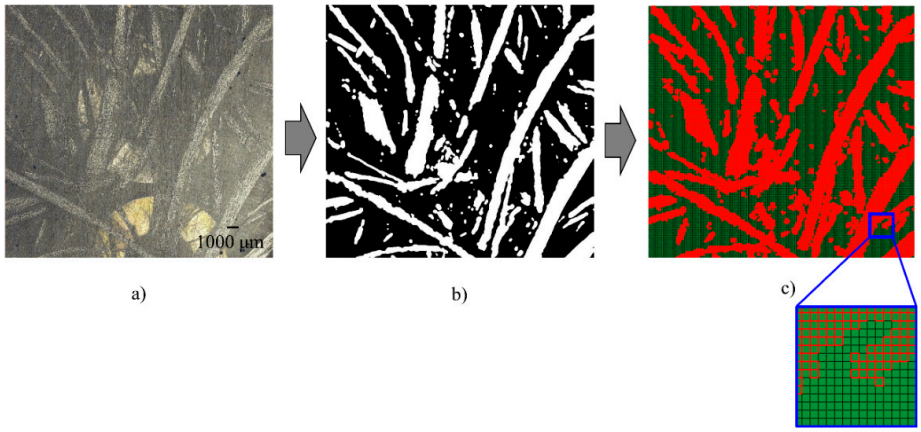

Figure 6. Image of representative microstructure and process analysis to assign a conforming mesh; (**a**) Original image collected through optical microscopy with a magnification of 100× showing the carbon fiber distribution from mixing Method 1, (**b**) Processed image after transferring to black and white and application of color threshold and blur and contrast filters the areal fiber fraction is ~33%, and (**c**) Conforming mesh to the microstructure based on color separation.

The next step was to assign the material properties to respective pixel groups. The properties of the material can be found in the 1st paragraph of the Materials and Methods section of this paper. Fibers and matrix are both modeled as elastic materials since they are examined within the linear elastic regime of the stress-strain curve. The simulation was performed on all samples collected for Method 1 set and Method 2 set by applying load in two principal directions (x axis and y axis considering the 2D plane of the field as a Cartesian coordinate system). If the mats are isotropic, they should yield comparable properties in both directions x and y as is hypothesized to result from the WL system.

The following boundary conditions, as seen in Figure 7, were used: (a) the displacement of the left edge was fully constrained (i.e., set to zero). The displacement of the lower left node in both x and y directions was also set to zero. A force in the x direction was applied to the right of the microstructure. (b) Displacement of the lower edge was set to zero. The displacement of the lower left node in both x and y directions was also set to zero. A force in the y direction was applied to the top of the microstructure.

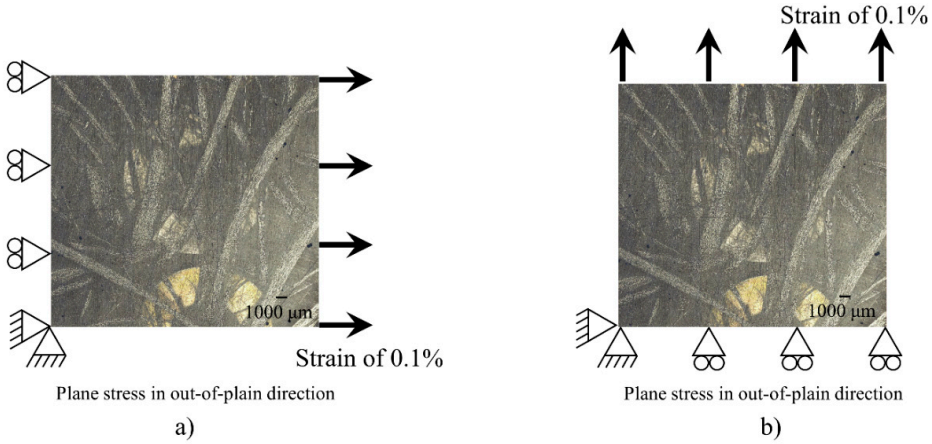

Figure 7. Boundary and loading condition for one of the original images collected through optical microscopy with a magnification of 100×. This sample areal fiber fraction is ~33%; (**a**) Left boundary fixed, lower left and bottom node fixed and constant force applied from the right hand side to cause a strain of 0.1% in the x axis direction in a Cartesian coordinate system, and (**b**) Lower boundary fixed, lower left and bottom node fixed and constant force applied from the top side to cause a strain of 0.1% in the y axis direction in a Cartesian coordinate system.

3. Results and Discussion

3.1. OOF Analysis Results for Isotropy Validation

The goal of this computational approach is to validate the isotropy of the WL mats. In general, the mats were assumed to be isotropic in nature as the WL system generates random orientation for the fibers in the mats. Isotropy is defined by having equal properties in multiple direction, in a way that the ratio of one property such as Young's modulus, measured in two orthogonal directions, should yield a value of 1. Table 1 displays the results of the FEA simulation and the ratio of Young's modulus calculated by the FEA analysis performed in ABAQUS 2018 – HF5 for the two principal directions of the 2D plane of the images. From these ratios, Method 2 samples are seen to have higher isotropy over those produced using Method 1. Figure 8 shows an example of the FEA simulation, where the fibers in the loading direction are highlighted in red as the primary stress bearing elements, while the fibers in normal direction to the load are indicated in the lower stress colder colors based on the Von-mises scale.

Table 1. Tensile Modulus in GPa as predicted by the OOF based FEA study.

Sample	Dir-X	Dir-Y	Ratio (x/y)	Sample	Dir-X	Dir-Y	Ratio (x/y)
M11	9.4	13.2	0.7	M21	15.0	16.5	0.9
M12	11.1	33.6	0.3	M22	9.2	11.8	0.8
M13	15.2	13.0	1.2	M23	9.5	8.4	1.1

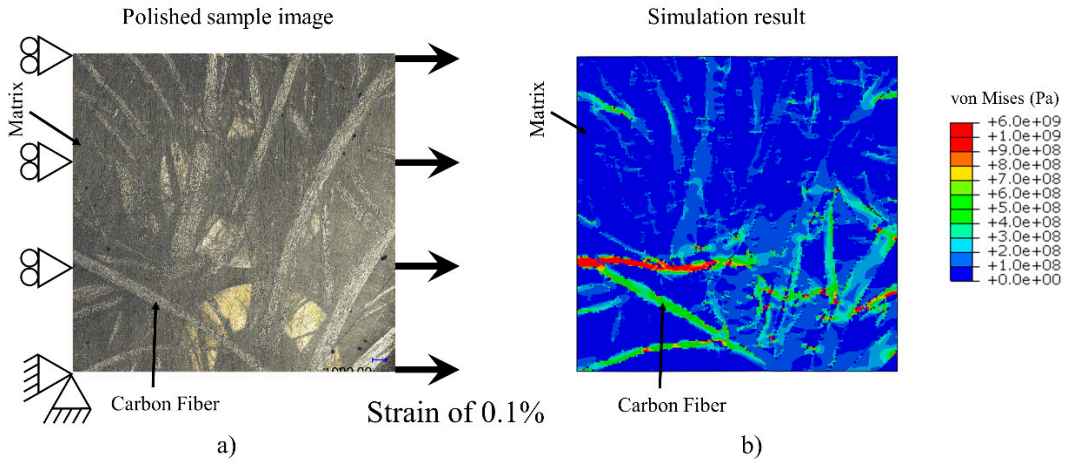

Figure 8. FEA simulation example showing (**a**) the original microstructure microscope image with the loading direction and (**b**) the fibers in the loading direction, bear the load and highlighted in warm colors. While the fibers that are perpendicular to the load direction remain in cold colors as they do not contribute to carrying the load.

3.2. Experimental Results

Table 2 summarizes the average tensile properties with respect to the weight fractions for Method 1 and Method 2 plates, respectively. 90% of the tensile samples failed in AGM (angled, gage, middle) mode and 10% in LGM (lateral, gage, middle). Table 3 summarizes normalized average tensile properties for each method in respect to unified weight fraction of 33%. The normalized values were calculated based on a linearized fit of the properties based on neighboring weight fraction. It must be noted that such fit will not be valid for difference of weight fraction above 5% between the considered samples for normalization. The linearized fitting equation is [33]:

$$Normalized\ value = test\ value * \frac{Chosen\ weight\ fraction}{weight\ fraction\ of\ test\ specimen} \quad (7)$$

Table 2. Experimental vs. theoretical tensile modulus (E) and ultimate tensile strength (σ) for individual plates. Where the nomenclature Mi Pj, indicates the Method number through i and the plate number through j.

Plate	W_f%	$E_{Experimental}$ (GPa)	STDE (GPa)	$E_{Theoretical}$ (GPa)	% Out of Theoretical	$\sigma_{Experimental}$ (MPa)	STDE (MPa)	$\sigma_{Theoretical}$ (MPa)	% Out of Theoretical
M1 P1	35	22	2	28	77	128	31	230	56
M1 P2	39	20	3	32	64	106	21	239	44
M1 P3	37	20	7	30	66	149	36	234	64
M2 P1	30	19	3	24	79	168	17	217	77
M2 P2	29	19	3	23	83	141	19	214	66
M2 P3	28	20	2	23	88	152	15	211	72

Table 3. Normalized average tensile properties for each method based on unified, normalized, fiber weight fraction of 33%.

Method	W_f% Average	$E_{Experimental}$ (GPa)	$E_{Theoretical}$ (GPa)	% Out of Theoretical	$\sigma_{Experimental}$ (MPa)	$\sigma_{Theoretical}$ (MPa)	% Out of Theoretical
M1	33	19	27	71	114	225	51
M2	33	22	27	83	173	225	77

Figure 9 compares the average experimental tensile Young's modulus of each plate to the theoretical modulus calculated using Halpin–Tsai equations [29] with respect to their fiber volume fraction. Since each set contained three plates, the average values presented in Figure 9 form a cluster distribution of data points. Analysis of the data cluster distribution presents higher control and repeatability of fiber weight content with composites made using Method 2 mats, with the three plates having 28%, 29% and 30% fiber volume ratios. The composites made with Method 1 mats had larger fiber weight content distribution at 35%, 39% and 37% for plates M1-P1, M1-P2, and M1-P3, respectively. This is attributed to the imbalance of fiber distribution in each layer, resulting in unequal fiber weight fractions in the various locations of the plates. This is reflected in the low standard deviation of 3% in Method 2 for fiber weight content, while for Method 1 the fiber weight content standard deviation was above 10%.

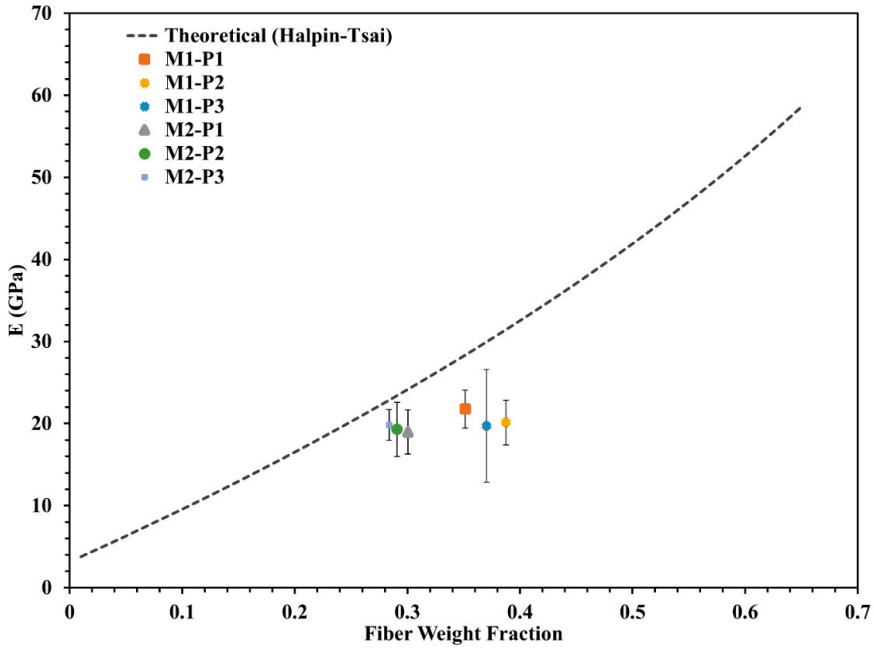

Figure 9. Average tensile modulus versus fiber weight fraction of each plate in both sets of Method 1 and Method 2. The blue line indicates the theoretical value calculated using the Halpin-Tsai equations.

The improvement of fiber distribution had direct correlation with an increase of Young's modulus experimental value obtained through Method 2 that was only 17% below the calculated theoretical value for a composite at the same fiber weight ratio. The imbalanced fiber distribution in Method 1 mats lead to average experimental values that are 32% below the calculated theoretical one for a composite of the same fiber weight content.

Figure 10 represents the tensile strength comparison between theoretical and experimental values for the plates of both sets. In Method 1, plates had a standard deviation of 21, 31 and 36 MPa (valued at 20%, 24.2% and 24%, respectively). Method 2 plates showed narrower standard deviation at 15, 17 and 19 MPa (valued at 10%, 14% and 9.8%). The cluster of the average tensile strength from samples of Method 1 showed a wider spread due to variability in weight content, and an average difference of 46% from theoretical value. The average cluster for Method 2 was closer to the theoretical value, with only a 28% difference. Such differences can be attributed to voids in the samples. The microstructure dependency plays an important role toward the deviation from theory (which assumes perfect isotropic material). Still, samples produced through Method 2 mats demonstrated a narrower standard deviation that did not surpass 10% between themselves, while the standard deviation for samples produced through Method 1 mats was higher than 20% when comparing between all three plates. These results were in accordance with the findings of the tensile modulus for individual samples collected from plates produced using mats from both methods.

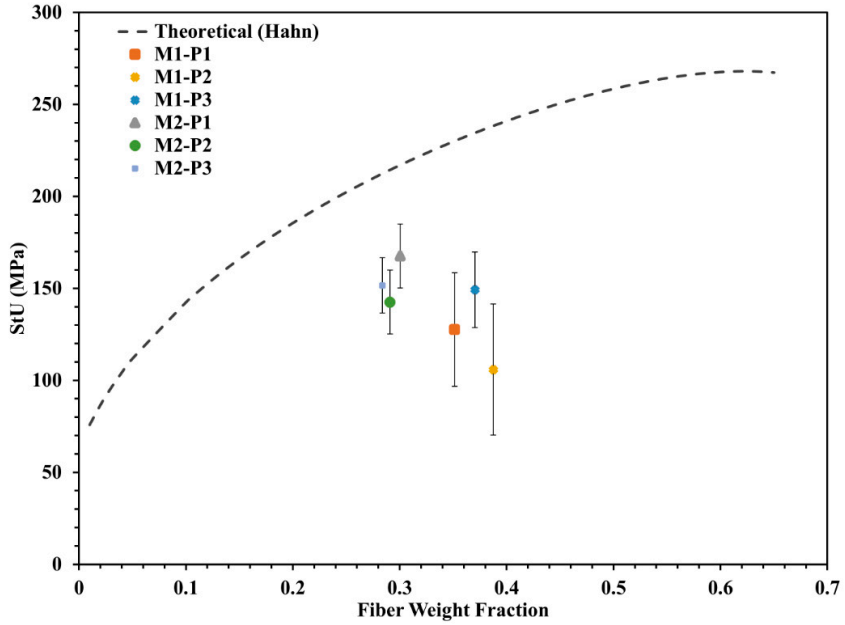

Figure 10. Average tensile strength vs. the fiber fraction weight of each of the plates from the sets of each method. The blue curve represents the theoretical value calculated based on the Hahn's equation.

Figure 11 shows the normalized tensile values with respect to a unified fiber weight fraction of 33% as presented in Table 3. This bar graph clarifies the improved performance of Method 2 over Method 1 by 16% in Young's modulus value and 52% in ultimate tensile strength. Optimal fiber distribution in Method 2 resulted in closing the gap with the theoretical values as well, with 10% improvement toward theoretical Young's modulus based on the Halpin–Tsai prediction, and a 26% improvement in tensile strength based on the Hahn's approach [32].

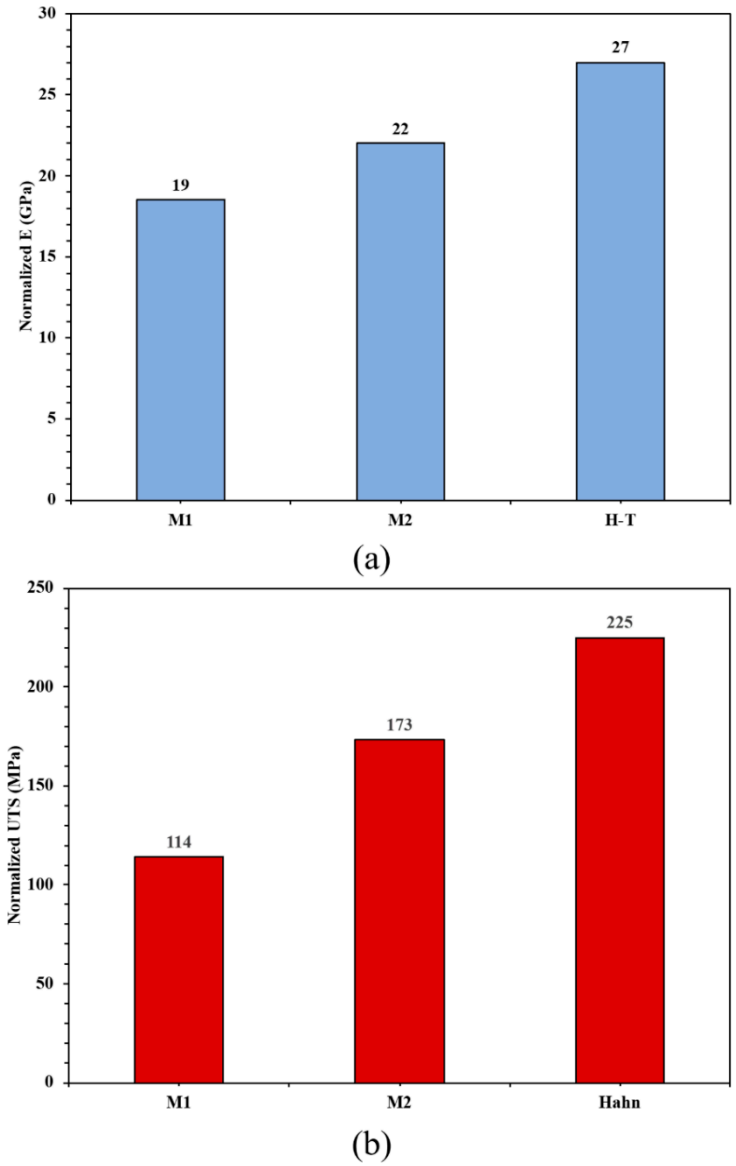

Figure 11. Normalized tensile properties for each method in respect to a unified fiber weight fraction of 33%. Method 2 shows significant improvement in performance over Method 1 both in; (**a**) Tensile modulus by 16%, and (**b**) Tensile strength by 52%.

Figure 12 shows SEM images of the fracture surface of the tensile samples. It is clear from Figure 12a that there is significant fiber grouping due to lack of proper dispersion in Method 1 and significant fiber pullout. On the other hand, Figure 12b presents a clean break surface with more fiber distribution due to innovation of fiber dispersion in Method 2.

Table 4 summarizes the average flexural properties, weight fractions, and void content for the Method 1 and Method 2 plates, respectively. Table 5 summarizes normalized flexural properties with respect to a unified fiber weight fraction of 33% for the plates.

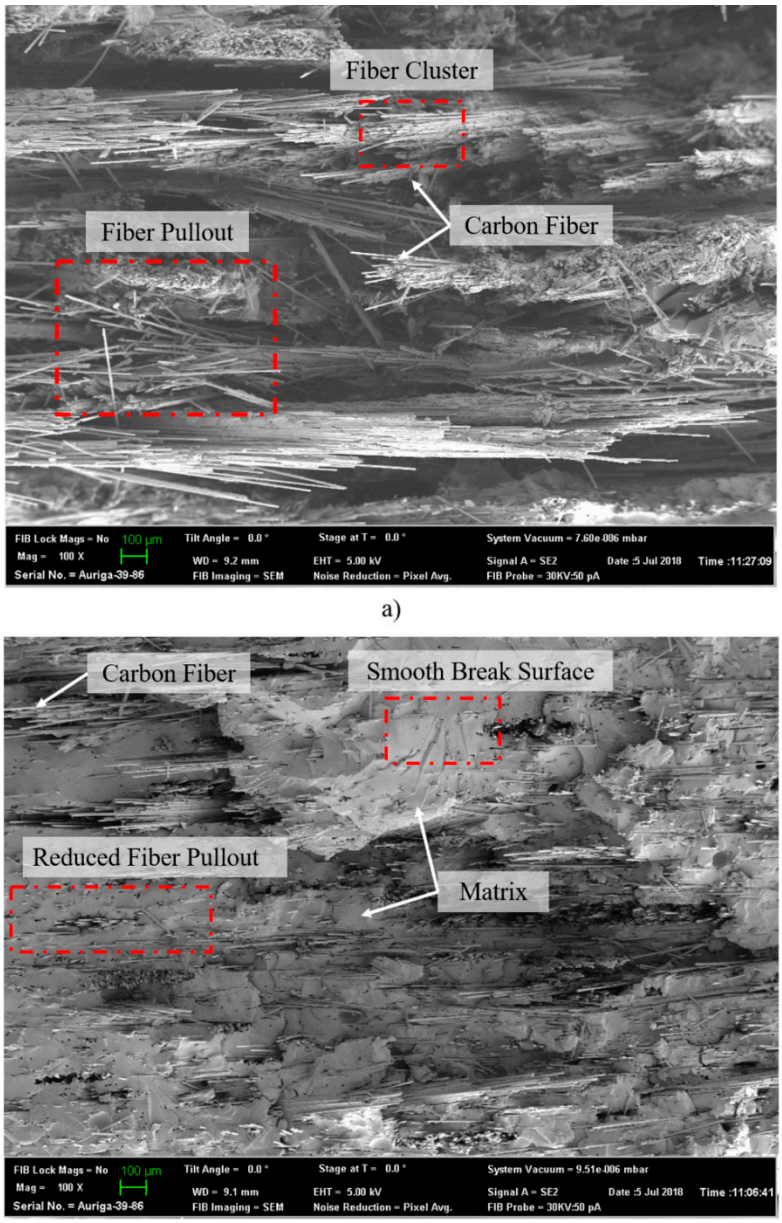

Figure 12. SEM images for selected break surface showing fiber random orientation and dispersion level for; (**a**) Method 1 sample break surface showing high density of bundle fibers, a sign of non-optimal dispersion, and (**b**) Method 2 sample break surface showing a clean area, a sign of optimal fiber dispersion.

Table 4. Experimental flexural results for the CF/Epoxy plates produced with WL-CF mats from Method 1 and Method 2 of nonwoven production.

Plate	W_f%	Flex Modulus (GPa)	STDE (GPa)	STDE (%)	Flex Strength (MPa)	STDE (MPa)	STDE (%)
M1 P1	35	14	6	46	252	85	34
M1 P2	39	13	3	25	242	43	18
M1 P3	37	13	3	22	241	43	18
M2 P1	30	12	1	6	243	23	10
M2 P2	29	12	2	17	239	38	16
M2 P3	28	12	1	11	234	22	10

Table 5. Normalized average flexural values for the plates from each method at a unified fiber weight fraction of 33%.

Method	W_f%	Flex Modulus (GPa)	Flex Strength (MPa)
M1	33	12	219
M2	33	14	270

Figure 13 shows the variance of the flexural modulus and strength in each method and a comparison between the normalized results of both methods. The normalized data for a normalized fiber weight fraction of 33% shows a significant increase in flexural modulus and strength of 17% and 23%, respectively, in Method 2 over Method 1. The other significant difference lies in the standard deviation for the individual plates where Method 2 plates have a variance of 6%, 17% and 11% while Method 1 plates have a variance of 46%, 25% and 22%.

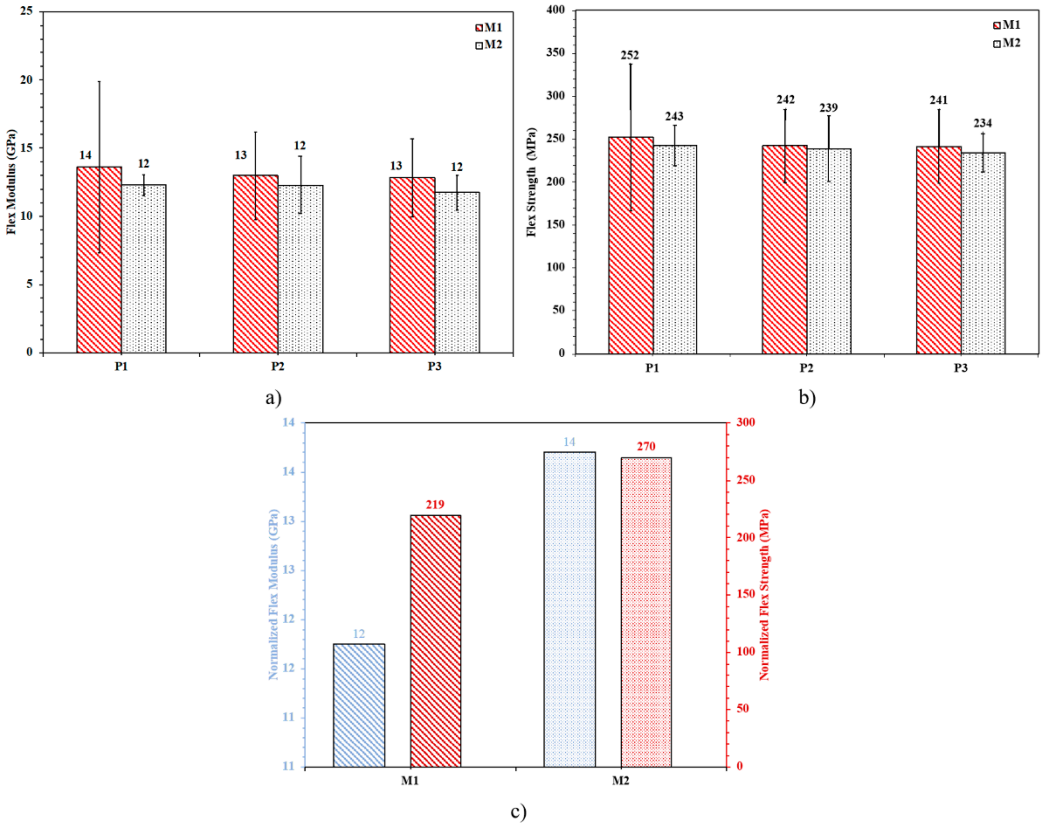

Figure 13. Flexural data for; (**a**) Flex modulus for Method 1 and Method 2 plates, (**b**) Flex strength for Method 1 and Method 2 plates, (**c**) Normalized average flex modulus and strength for Method 1 Set versus Method 2 set for a unified fiber weight fraction of 33%, the superiority of Method 2 is reflected by the positive slope of the trendline between the calculated values.

Table 6 and Figure 14 summarizes the average ILSS for each individual plate from both sets and Table 7 shows the average of each set. Figure 15 highlights the performance in ILSS for both methods, with a bar graph showing superiority of Method 2 over Method 1 by 15 MPa. It is hypothesized that with optimal filament dispersion, increased fiber surface area causes the improvement of the ILSS.

Table 6. Average ILSS of each individual plate from both sets.

Plate	W_f%	ILSS (MPa)	STDE (MPa)	STDE%
M1-P1	35	16.44	5.62	34
M1-P2	39	21.39	3.46	16
M1-P3	37	23.24	5.63	24
M2-P1	30	31.92	2.41	8
M2-P2	29	30.87	2.05	7
M2-P3	28	25.91	1.58	6

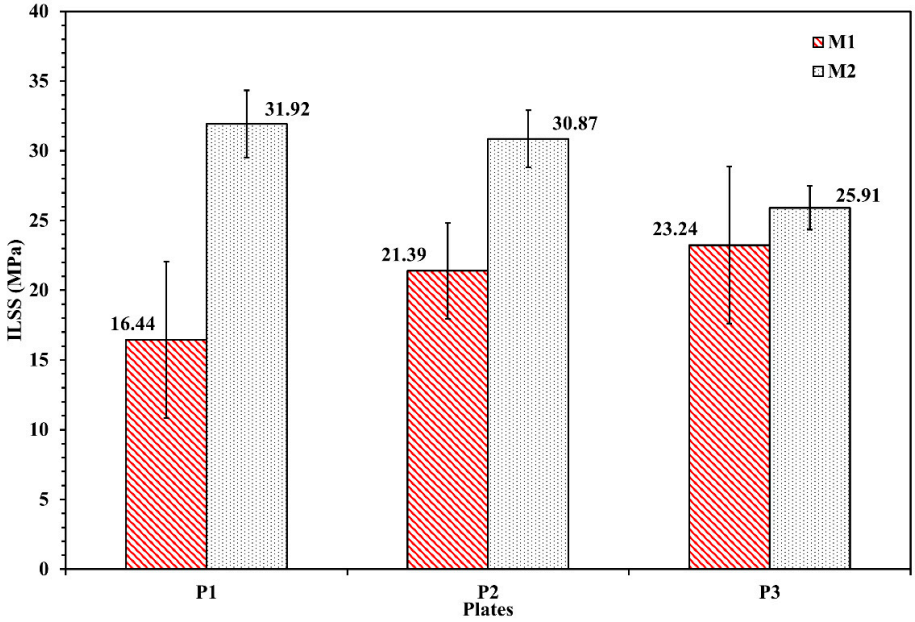

Figure 14. Average ILSS of each plate from both samples sets fabricated by Method 1 and Method 2; despite the superiority of fiber weight fraction in Method 1 plates, it is clear that Method 2 plates are outperforming Method 1 plates by values of 10%, to 90% with higher consistency in standard deviation.

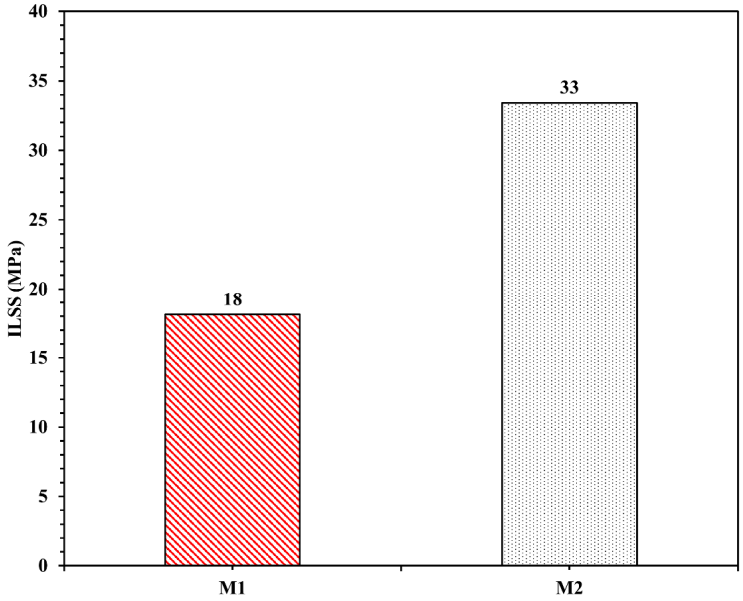

Figure 15. Normalized average ILSS of each set showing the improvement of 83% caused by optimal fiber dispersion in Method 2 when compared to Method 1.

Table 7. Normalized average ILSS values of each set for a unified fiber weight fraction of 33%.

Plates	W_f%	Normalized ILSS (MPa)
M1	33	18
M2	33	33

4. Conclusions

Two sets of composites were made from WL-CF nonwoven mats and were consolidated and tested for tensile, flex and ILSS. The mats of each set were prepared through the two mixing regimes, Method 1 and Method 2 presented in [5]. The composites' isotropy was validated by computational method through OOF. OOF demonstrated higher isotropy in composites made through Method 2 versus those made through Method 1, thanks to the optimal fiber dispersion achieved in Method 2. The tensile properties were analyzed and compared against the Halpin–Tsai predictions for Young's modulus and the Hahn's approach for ultimate tensile strength. The optimal fiber dispersion improved the values of Young's modulus by 16% from Method 1 and more closely aligned with the Halpin–Tsai prediction by 10%. The effect of optimal fiber dispersion in Method 2 reflected as well on the flexural properties, which increase by 17% and 23% for modulus and strength, respectively. As for the ILSS, Method 2 showed a superiority of 83%, which may be attributed to the uniform fiber distribution. With these findings it can be concluded that use of WL CF nonwoven mats produced by the innovative Method 2 proposed in [5] should be adopted for composites production. These optimized mats helped bridge the gap between theoretical and experimental values, enabling the design and fabrication of complex geometry parts with long discontinuous fibers through low-cost manufacturing techniques, such as out of autoclave methods and VARTM.

Author Contributions: Conceptualization, H.G., A.A.H. and U.K.V.; methodology, H.G., A.A.H.; software, S.K., J.A.; validation, H.G., A.A.H. and S.K.; formal analysis, H.G.; investigation, H.G.; resources, U.K.V.; data curation, H.G.; writing—original draft preparation, H.G.; writing—review and editing, H.G., A.A.H., S.K., J.A. and U.K.V.; visualization, H.G. and A.A.H; supervision, U.K.V.; project administration, H.G. and U.K.V.; funding acquisition, U.K.V. All authors have read and agreed to the published version of the manuscript.

Funding: The research was funded in part by the Office of Energy Efficiency and Renewable Energy (EERE), U.S. Department of Energy, under Award Number DE-EE0006926. Support from the Institute for Advanced Composites Manufacturing Innovation (IACMI-The Composites Institute is gratefully acknowledged.

Acknowledgments: The authors want to acknowledge and thank Stephen Langer from the Mathematical Software Group, at the National Institute of Standards and Technology (NIST) for providing access to the OOF software. His generous help made this work possible. This research was supported by the DOE Office of Energy Efficiency and Renewable Energy (EERE), Advanced Manufacturing Office and used resources at the Manufacturing Demonstration Facility, a DOE-EERE User Facility at Oak Ridge National Laboratory.

Conflicts of Interest: The authors declare no conflict of interest.

References

1. Pervaiz, M.; Panthapulakkal, S.; KC, B.; Sain, M.; Tjong, J. Emerging Trends in Automotive Lightweighting through Novel Composite Materials. *Mater. Sci. Appl.* **2016**, *7*, 26–38. [CrossRef]
2. Knopp, A.; Scharr, G. Tensile Properties of Z-Pin Reinforced Laminates with Circumferentially Notched Z-Pins. *J. Compos. Sci.* **2020**, *4*, 78. [CrossRef]
3. Chung, D.D.L. Review: Materials for vibration damping. *J. Mater. Sci.* **2001**, *36*, 5733–5737. [CrossRef]
4. Akonda, M.H.; Lawrence, C.A.; Weager, B.M. Recycled carbon fibre-reinforced polypropylene thermoplastic composites. *Compos. Part A Appl. Sci. Manuf.* **2012**, *43*, 79–86. [CrossRef]
5. Ghossein, H.; Hassen, A.A.; Paquit, V.; Love, L.J.; Vaidya, U.K. Innovative Method for Enhancing Carbon Fibers Dispersion in Wet-Laid Nonwovens. *Mater. Today Commun.* **2018**, *17*, 100–108. [CrossRef]
6. Yeole, P.; Ning, H.; Hassen, A.A.; Vaidya, U.K. The Effect of Flocculent, Dispersants, and Binder on Wet-laid Process for Recycled Glass Fiber/PA6 Composite. *Polym. Polym. Compos.* **2018**, *26*(3), 259–269. [CrossRef]
7. Lu, L.; Xing, D.; Xie, Y.; Teh, K.S.; Zhang, B.; Chen, S.M.; Tang, Y. Electrical conductivity investigation of a nonwoven fabric composed of carbon fibers and polypropylene/polyethylene core/sheath bicomponent fibers. *Mater. Des.* **2016**, *112*, 383–391. [CrossRef]
8. Deng, Q.; Li, X.; Zuo, J.; Ling, A.; Logan, B.E. Power generation using an activated carbon fiber felt cathode in an upflow microbial fuel cell. *J. Power Sources* **2010**, *195*, 1130–1135. [CrossRef]
9. Meng, C.; Liu, C.; Fan, S. Flexible carbon nanotube/polyaniline paper-like films and their enhanced electrochemical properties. *Electrochem. Commun.* **2009**, *11*, 186–189. [CrossRef]
10. Shen, L.; Wang, J.; Xu, G.; Li, H.; Dou, H.; Zhanga, X. $NiCo_2S_4$ nanosheets grown on nitrogen-doped carbon foams as an advanced electrode for supercapacitors. *Adv. Energy Mater.* **2015**, *5*, 2–8. [CrossRef]
11. Straumit, I.; Lomov, S.V.; Wevers, M. Quantification of the internal structure and automatic generation of voxel models of textile composites from X-ray computed tomography data. *Compos. Part A Appl. Sci. Manuf.* **2015**, *69*, 150–158. [CrossRef]
12. Wan, Y.; Takahashi, J. Tensile and compressive properties of chopped carbon fiber tapes reinforced thermoplastics with different fiber lengths and molding pressures. *Compos. Part A Appl. Sci. Manuf.* **2016**, *87*, 271–281. [CrossRef]
13. Wan, Y.; Straumit, I.; Takahashi, J.; Lomov, S.V. Micro-CT analysis of internal geometry of chopped carbon fiber tapes reinforced thermoplastics. *Compos. Part A Appl. Sci. Manuf.* **2016**, *91*, 211–221. [CrossRef]
14. Tseng, H.; Chang, R.; Hsu, C. Numerical prediction of fiber orientation and mechanical performance for short/long glass and carbon fiber-reinforced composites. *Compos. Sci. Technol.* **2017**, *144*, 51–56. [CrossRef]
15. Feraboli, P.; Kawakami, H.; Wade, B.; Gasco, F.; DeOto, L.; Masini, A. Recyclability and reutilization of carbon fiber fabric/epoxy composites. *J. Compos. Mater.* **2011**, *46*, 1459–1473. [CrossRef]
16. Caba, A.C.; Loos, A.C.; Batra, R.C. Fiber-fiber interactions in carbon mat thermoplastics. *Compos. Part A Appl. Sci. Manuf.* **2007**, *38*, 469–483. [CrossRef]
17. Evans, A.D.; Qian, C.C.; Turner, T.A.; Harper, L.; Warrior, N.A. Flow characteristics of carbon fibre moulding compounds. *Compos. Part A Appl. Sci. Manuf.* **2016**, *90*, 1–12. [CrossRef]
18. Selezneva, M.; Lessard, L. Characterization of mechanical properties of randomly oriented strand thermoplastic composites. *J. Compos. Mater.* **2016**, *50*, 2833–2851. [CrossRef]
19. Amaro, A.M.; Reis, P.N.B.; Santos, J.B.; Santos, M.J.; Neto, M.A. Effect of the electric current on the impact fatigue strength of CFRP composites. *Compos. Struct.* **2017**, *182*, 191–198. [CrossRef]
20. Thomason, J.L. The influence of fibre length and concentration on the properties of glass fibre reinforced polypropylene: Injection moulded long and short fibre PP. *Compos. Part A Appl. Sci. Manuf.* **2002**, *33*, 1641–1652. [CrossRef]
21. Langer, S.A.; Fuller, E.R.; Carter, W.C. OOF: An image-based finite-element analysis of material microstructures. *Comput. Sci. Eng.* **2001**, *3*, 15–23. [CrossRef]
22. Reid, A.C.E.; Lua, R.C.; García, R.E.; Coffman, V.R.; Langer, S.A. Modelling Microstructures with OOF2. *Int. J. Mater. Prod. Technol.* **2009**, *35*, 361. [CrossRef]
23. Dong, Y.; Bhattacharyya, D. Morphological-image analysis based numerical modelling of organoclay filled nanocomposites. *Mech. Adv. Mater. Struct.* **2010**, *17*, 534–541. [CrossRef]
24. Dong, Y.; Bhattacharyya, D.; Hunter, P.J. Characterisation and Object-Oriented Finite Element Modelling of Polypropylene/Organoclay Nanocomposites. *Key Eng. Mater.* **2007**, *334–335*, 841–844. [CrossRef]

25. Cannillo, V.; Esposito, L.; Pellicelli, G.; Sola, A.; Tucci, A. Steel particles–porcelain stoneware composite tiles: An advanced experimental–computational approach. *J. Eur. Ceram. Soc.* **2010**, *30*, 1775–1783. [CrossRef]
26. Bakshi, S.R.; Patel, R.R.; Agarwal, A. Thermal conductivity of carbon nanotube reinforced aluminum composites: A multi-scale study using object oriented finite element method. *Comput. Mater. Sci.* **2010**, *50*, 419–428. [CrossRef]
27. Coffman, V.R.; Reid, A.C.E.; Langer, S.A.; Dogan, G. OOF3D: An image-based finite element solver for materials science. *Math. Comput. Simul.* **2012**, *82*, 2951–2961. [CrossRef]
28. Goel, A.; Chawla, K.K.; Vaidya, U.K.; Chawla, N.; Koopman, M. Two-dimensional microstructure based modelling of Young's modulus of long fibre thermoplastic composite. *Mater. Sci. Technol.* **2008**, *24*, 864–869. [CrossRef]
29. Affdl, J.C.H.; Kardos, J.L. The Halpin-Tsai equations: A review. *Polym. Eng. Sci.* **1976**, *16*, 344–352. [CrossRef]
30. Shokrieh, M.M.; Moshrefzadeh-Sani, H. On the constant parameters of Halpin-Tsai equation. *Polymer* **2016**, *106*, 14–20. [CrossRef]
31. Mallick, P.K. *Fiber-Reinforced Composites: Materials, Manufacturing, and Design*, 3rd ed.; CRC Taylor & Francis Group: Philadelphia, PA, USA, 2007.
32. Hahn, H.T. On Approximations for Strength of Random Fiber Composites. *J. Compos. Mater.* **1975**, *9*, 316–326. [CrossRef]
33. DOF. *Composite Materials Handbook-MIL 17*, 1st ed.; Taylor & Francis: New York, NY, USA, 1999. [CrossRef]